Stretch-tuneable dielectric mirrors and optical microcavities

Mathias Kolle, Bo Zheng, Nicholas Gibbons, Jeremy J. Baumberg, and Ullrich Steiner*

Cavendish Laboratory, University of Cambridge, Cambridge, CB3 0HE, UK

*u.steiner@phy.cam.ac.uk

Abstract: We demonstrate how tuneable Distributed Bragg Reflectors (DBRs) and resonant micro-cavities can be built by a scalable layer assembly of the transparent utility rubbers polydimethylsiloxane and polystyrene-polyisoprene. Stretching the devices by more than 60% leads to an affine contraction of the layer thicknesses thereby tuning both DBR and cavity modes across the entire visible spectrum. Such rapidly- and reversibly- stretch-tuneable cavities can be used in tuneable micro-lasers and for quantitative optical strain sensing applications.

OCIS codes: (220.4241) Nanostructure fabrication; (230.1480) Bragg reflectors; (350.4238) Nanophotonics and photonic crystals.

References and links

1. M. Born and E. Wolf, *Principles of Optics*, (Cambridge University Press, 2005).
2. F. Abeles, "Recherches sur la propagation des ondes électromagnétiques sinusoïdales dans les milieux stratifiés. Application aux couches minces," Ann. Phys. (series 12) **5**, 596–640 (part I), 706–784 (part II) (1950).
3. O.S. Heavens, *Optical properties of thin solid films*, (Dover Publications, 1965).
4. Y. Fink, J. N. Winn, S. Fan, C. Chen, J. Michel, J. D. Joannopoulos & E.L. Thomas, "A Dielectric Omnidirectional Reflector," Science **282**, 1679–1682 (1998).
5. D. L. Huffaker and D. G. Deppe, "Low threshold vertical-cavity surface-emitting lasers based on high contrast distributed Bragg reflectors," Appl. Phys. Lett. **70**, 1781–1783 (1997).
6. E. F. Schubert, Y. H. Wang, A. Y. Cho, L. W. Tu, and G. J. Zydzik, "Resonant cavity light emitting diode," Appl. Phys. Lett. **60**, 921–923 (1992).
7. H. Jiang, E. Johnson, K. Eyink, J. Grant, D. Tomlin, and T. Bunning, "Plasma Polymerized Multi-Layered Photonic Films," Chem. Mater. **15**, 340–347 (2003).
8. M. F. Weber, C. A. Stover, L. R. Gilbert, T. J. Nevitt, and A. J. Ouderkirk, "Giant Birefringent Optics in Multilayer Polymer Mirrors," Science **287**, 2451–2456 (2000).
9. T. Komikado, A. Inoue, K. Masuda, T. Ando, and S. Umegaki, "Multi-layered mirrors fabricated by spin-coating organic polymers," Thin Solid Films **515**, 3887–3892 (2007).
10. A. C. Edrington, A. M. Urbas, P. DeRege, C. X. Chen, T. M. Swager, N. Hadjichristidis, M. Xenidou, L. J. Fetters, J. D. Joannopoulos, and Y. Fink, "Polymer-based photonic crystals," Adv. Mater. **13**(6), 421–425 (2001).
11. S. Setzu, P. Ferrand, and R. Romestain, "Optical properties of multilayered porous silicon," Mater. Sci. Eng. B **69**, 34–42 (2000).
12. W. Gellermann, M. Kohmoto, . Sutherland, and P.C. Taylor, "Localization of light wave in Fibonacci dielectric multilayers," Phys. Rev. Lett. **72**(5), 633–636 (1994).
13. R. P. Stanley, R. Houdre, U. Oesterle, M. Gailhanou, and M. Ilegems, "Ultrahigh finesse microcavity with distributed Bragg reflectors," Appl. Phys. Lett. **65**(15), 1883–1885 (1994).
14. R. Langer, A. Barski, J. Simon, N. T. Pelekanos, O. Konovalov, and R. Andre, "High-reflectivity GaN/GaAlN Bragg mirrors at blue/green wavelengths grown by molecular beam epitaxy," Appl. Phys. Lett. **74** 3610–3612 (1999).
15. L. Martinu and D. Poitras, "Plasma deposition of optical films and coatings: A review," J. Vac. Sci. Tech. A **18**, 2619–2645 (2000).
16. F. Serra, M. A. Matranga, Y. Ji, and E. M. Terentjev, "Single-mode laser tuning from cholesteric elastomers using a notch band-gap configuration," Opt. Express **18**, 575–581 (2010).

#121929 - $15.00 USD Received 23 Dec 2009; revised 27 Jan 2010; accepted 3 Feb 2010; published 17 Feb 2010

17. Y. Hirota, Y. Ji, F. Serra, A. R. Tajbakhsh, and E. M. Terentjev, "Effect of crosslinking on the photonic bandgap in deformable cholesteric elastomers," Opt. Express **16**, 5320–5331 (2008).
18. P. Cicuta, A. R. Tajbakhsh, and E. M. Terentjev, "Photonic gaps in cholesteric elastomers under deformation," Phys. Rev. E **70**, 011703 (2004).
19. L. Domash, M. Wu, N. Nemchuk, and E. Ma, "Tunable and switchable multiple-cavity thin film filters," J. Lightwave Technol. **22**(1), 126–135 (2004).
20. W. Mönch, J. Dehnert, O. Prucker, J. Rühe, and H. Zappe, "Tunable Bragg filters based on polymer swelling," Appl. Opt. **45**, 4284–4290 (2006).
21. Y. Kang, J. J. Walish, T. Gorishnyy, and E. L. Thomas, "Broad-wavelength-range chemically tunable block-copolymer photonic gels," Nat. Mater. **6**, 957–960 (2007).
22. M. Sandrock, M. Wiggins, J. S. Shirk, H. Tai, A. Ranade, E. Baer, and A. Hiltner, "A widely tunable refractive index in a nanolayered photonic material," Appl. Phys. Lett. **84**, 18, 3621–3623 (2004).
23. M. Kimura, K. Okahara, and T. Miyamoto, "Tunable multilayer-film distributed-Bragg-reflector filter," J. Appl. Phys. **50**, 1222–1225 (1979).
24. S. Shojaei-Zadeh, S. R. Swanson, and S. L. Anna, "Highly uniform micro-cavity arrays in flexible elastomer film," Soft Matter **5**, 743–746 (2009).
25. O. L. J. Pursiainen, J. J. Baumberg, H. Winkler, B. Viel, P. Spahn, and T. Ruhl, "Nanoparticle-tuned structural color from polymer opals," Opt. Express **15**, 9553–9561 (2007).
26. J. Li, Y. Wu, J. Fu, Y. Cong, J. Peng, and Y. Han, "Reversibly strain-tunable elastomeric photonic crystals," Chem. Phys. Lett. **390**(1-3), 285–289 (2004).
27. N. Gibbons, J.J. Baumberg, C.L. Bower, M. Kolle, amd U. Steiner, "Scalable Cylindrical Metallo-dielectric Metamaterials," Adv. Mater. **21**, 3933 (2009).
28. A. V. Kavokin and J. J. Baumberg, '*Microcavities*, (Oxford University Press, 2007).
29. W. Caseri, "Nanocomposites of polymers and metals or semiconductors: Historical background and optical properties," Macromol. Rapid Commun. **21**, 705–722 (2000).
30. M. Rubinstein and R. H. Colby, *Polymer Physics*, (Oxford University Press, 2003).
31. A. Hotta, S. M. Clarke and E. M. Terentjev, "Stress Relaxation in Transient Networks of Symmetric Triblock Styrene-Isoprene-Styrene Copolymer," Macromolecules **35**, 271-277 (2000)
32. R. C. Pennington, G. D'Alessandro, J. J. Baumberg, and M. Kaczmarek, "Spectral properties and modes of surface microcavities," Phys. Rev. A **79**, 043822 (2009).

1. Introduction

Periodic multilayers of transparent dielectrics are among the most common optical elements [1–3], used to produce high reflectivity Distributed Bragg Reflectors (DBRs) [4], broadband beamsplitters, optical filters, and optical microcavities. The latter are important for light emission in vertical cavity semiconductor lasers [5] and resonant cavity light emitting diodes [6]. While the manufacture of polymeric DBRs has been reported [4, 7–10], the greatest drawbacks of multilayer optical components is their lack of tuneable performance due to their composition from rigid layers [11–15]. Recently, tuneable photonic band-gap materials and lasing devices have been realised using cholesteric liquid crystal elastomers [16–18]. Here we demonstrate fabrication of entirely elastomeric multilayer dielectric stacks, which can be stretched by over 60% to achieve rapid, reversible wavelength tuning.

Typical tuning schemes for multilayer optical components use thermal expansion (which limits the accessible wavelength ranges [19]) or solvent-swelled expansion, which predominantly acts on only one of the layer types degrading the optical performance [20]. Promising recent block co-polymer-based multilayer mirrors operate only in liquid environments, thus producing significant additional challenges [21]. All of these mechanisms are slow and limited by solvent or thermal diffusion into the layer stacks. Conversely, compression of multilayer stacks produces only limited wavelength tuning [22, 23], while high reflectivity 3D elastomeric photonic crystals composed of spheres cannot yet be simply fabricated on large scales [24–26]. Our technique, on the other hand, relies on the direct deposition of only a single polymer bilayer which is sequentially stacked to form high quality DBRs and microcavities. By using two polymer rubbers, the resulting optical structures are highly flexible. Such thin flexible mirrors and cavities can be assembled into unusual configurations, are easily scalable to large-scale manufacture, and promise high quality factor performance without compromising tuning.

#121929 - $15.00 USD Received 23 Dec 2009; revised 27 Jan 2010; accepted 3 Feb 2010; published 17 Feb 2010

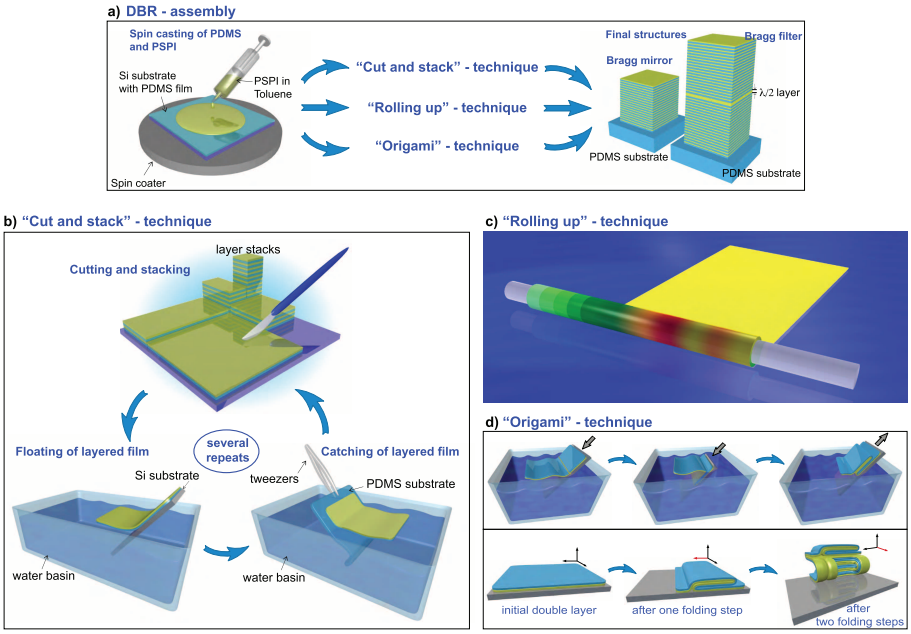

Fig. 1. **Schematic DBR assembly: (a)** Initial double layer, produced by spin-cast PDMS film followed by thermal annealing and spin-cast PSPI film on top, produces DBRs efficiently via three different routes. **(b)** "Cut and stack" technique: repeated cutting and floating followed by the stacking of layered films on top of each other. **(c)** "Roll-up" technique: double layer floated onto a water surface is rolled up onto a flexible transparent rod. **(d)** "Origami" technique: based on three-step folding cycle leading to a *z*-fold. Lower box shows initial bi-layer, and stack after one and two folding cycles. Red arrows indicate folding direction.

2. Sample preparation and experimental setup

Tuneable DBRs (often called 1D photonic crystals) are constructed from alternating layers of high and low refractive index layers, where for each layer in the stack

$$\bar{\lambda} = 4d_i\sqrt{n_i^2 - \sin^2\theta} \tag{1}$$

with $\bar{\lambda}$ being the central reflection stopband wavelength, θ is the angle of light incidence and d_i, n_i are the thickness and refractive index of the i-th layer. The multilayer structures here are manufactured from two commodity elastomers, a silicone rubber, polymethylsiloxane (PDMS, Dow Corning - Sylgard 184) and an elastic tri-block-copolymer which consists of polyisoprene containing a 22 wt% minority polystyrene phase (PSPI, Sigma Aldrich). Both materials are transparent. The Poisson ratio, a measure for the compression of an object perpendicular to the stretching direction, is 0.5 for PDMS and PSPI as for many rubbers. Consequently, applying an in-plane deformation to a PDMS - PSPI multilayer results in a proportional change in layer thickness. The refractive indices of thin PDMS and PSPI films are measured by ellipsometry to give $n_{\mathrm{PDMS}} = 1.41 \pm 0.02$ and $n_{\mathrm{PSPI}} = 1.54 \pm 0.02$.

Fabrication of the stretch-tuneable optical elements is shown in Fig. 1. PDMS is dissolved in heptane and spun onto a silicon substrate. Annealing in an oven at 120 °C for one hour leads to crosslinking of the PDMS which makes it resistent to toluene, the solvent used for the PSPI

#121929 - $15.00 USD Received 23 Dec 2009; revised 27 Jan 2010; accepted 3 Feb 2010; published 17 Feb 2010

copolymer. PSPI is subsequently spun onto the PDMS layer. The resulting layer thicknesses (determined by atomic force microscopy (AFM) and ellipsometry) of $d_{\mathrm{PDMS}} = 165 \pm 10\,\mathrm{nm}$ and $d_{\mathrm{PSPI}} = 295 \pm 10\,\mathrm{nm}$ are optimized to maximize the DBR reflectivity in the red part of the visible spectrum. The micro-phase separation of the polystyrene component in the PSPI leads to nanoscopic glassy minority domains in a polyisoprene matrix, which act as cross-links, rendering the curing of the polyisoprene rubber unnecessary.

Assembly into multilayer stacks can proceed via several routes. In the simplest process, the double layer is subsequently cut into small sections of $5\,\mathrm{mm} \times 10\,\mathrm{mm}$ on the silicon substrate. Pieces of double layer are released from the substrate by floating them onto a water surface and they are sequentially overlaid onto a PDMS rubber slab to form a multilayer. In this fashion a DBR consisting of 20 layers is assembled. In addition, a resonant multilayer microcavity consisting of two multilayer stacks enclosing a $\lambda/2$ PSPI cavity layer is realized. The film thicknesses in the resonant microcavity are $d_{\mathrm{PDMS}} \approx 150\,\mathrm{nm}$, $d_{\mathrm{PSPI}} \approx 250\,\mathrm{nm}$ and $d_{\mathrm{PSPI\ cavity}} \approx 295\,\mathrm{nm}$.

This assembly procedure is time-consuming as the number of layers scales linearly with the number of floating steps. Furthermore, the likelihood of introducing defects into the structure increases with every floating step. In order to minimise the number of production steps three other highly-scaleable, less defect-prone techniques were also developed.

2.1. "Cut and stack" technique

An improved variant of stack manufacture consists of cutting an initial stack of i layers in half and superposing one part onto the other to form a $2i$-layer stack [Fig.1(b)]. Starting with an initial double layer this repeated 'cut and stack' procedure leads to a stack of 128 layers in only six steps. More generally the number of layers l_c in a DBR stack varies as

$$l_c = 2^{c+1} \tag{2}$$

with c being the number of cut-and-stack operations.

2.2. "Roll-up" technique

This method proceeds from a double-layer film with the appropriate layer thicknesses d_1, d_2 [see Eq. (1)] that is floated onto a water surface. Subsequently the floating bi-layer is rolled up onto a transparent, stretchable, cylindrical or square rod made from polydimethylsiloxane (PDMS). The number of layers on the rod scales with the number of complete turns when rolling up the film [Fig.1(c)]. We also recently reported this technique for fabricating metallo-dielectric multilayer rolls [27].

2.3. "Origami" technique

Here the film is repeatedly folded onto itself. As with the cut-and-stack and roll-up methods, this technique proceeds from an initial polymer bilayer. However, here the thicknesses of the individual layers are one-half of the thicknesses required for DBR construction ($d_1/2$, $d_2/2$). Repeated folding of the entire stack onto itself leads to a multilayer stack with the number of individual layers increasing very rapidly with each folding operation. Sequential folding of the entire stack is achieved by a simple strategy: the slow immersion of a supported film partially releases the film onto the water surface up to a line where the film is physically fixed onto the substrate to prevent further release. By continuing to immerse the sample beyond this line, part of the floating film is redeposited onto the unreleased part of the double layer. Finally, slow retraction of the sample induces a second folding of the released film onto the folded part. In short, one folding cycle [displayed in the top of Fig. 1(d)] leads to a z-fold. The lower part of

#121929 - $15.00 USD Received 23 Dec 2009; revised 27 Jan 2010; accepted 3 Feb 2010; published 17 Feb 2010

Fig.1(d) shows the initial bi-layer film, a multilayer after one folding cycle and a stack after two folding cycles. In this method, the final DBR is terminated by half-layers on both surfaces. If required, this is easily fixed by floating individual half-layers onto the final stack. The main advantage of the origami technique is the way the overall layer number in the stack, l_f, scales with the number of folding operations, f, as

$$l_f = 3^f - 1. \tag{3}$$

These three techniques have the advantage of minimising the number of floating steps, reducing the likelihood of including defects (e.g. by dust particles) into the stack. The careful assembly of multilayers on the water surface or at the water meniscus prevents incorporation of air bubbles leading to defect-free areas of several square centimetres.

Although the presented samples are prototypes made by simple sequential films superposition, optimisation now in progress will allow larger area fabrication and potentially continuous roll-to-roll processes for the multilayer fabrication of elastomeric DBRs and cavities.

3. Cavity design and modelling

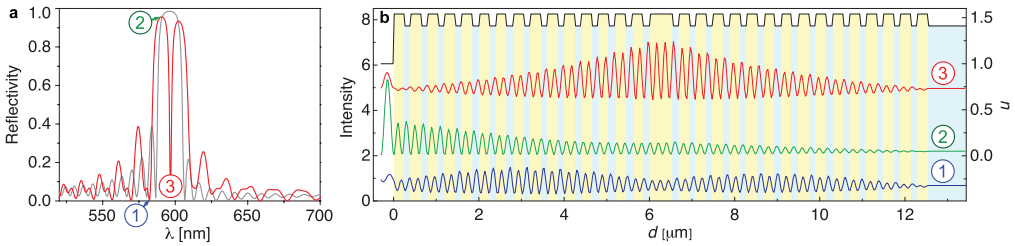

Fig. 2. **Simulated reflectivity spectra. (a)** Bragg mirror consisting of 15 double layers (black line) and a microcavity (red line) constructed from two 15 double layer DBRs surrounding a cavity spacer. **(b)** Field distributions in the cavity structure at 582 nm (1), 590 nm (2) and 597 nm (3), marked in **(a)**.

The optical performance of a fully elastomeric microcavity based on two stretchable DBRs surrounding a $\lambda/2$ spacer was simulated using a standard transfer matrix technique. The results of these simulations were used to determine optimal film thicknesses that were targeted in DBR manufacture. Figure 2 shows a reflectivity spectrum of a DBR structure (black line) made from 30 bilayers with thicknesses $d_1 = 250$ nm, $d_2 = 150$ nm and refractive indices $n_1 = 1.54$, $n_2 = 1.41$. The refractive indices of the superstrate and the substrate are 1.0 and 1.41, respectively. The red line is the calculated reflectivity of a microcavity consisting of two DBR stacks enclosing a cavity layer of thickness $d_c = 295$ nm and refractive index $n_c = 1.54$. Figure 2(b) shows calculated field distributions of the light in the cavity for the three different wavelengths marked in Fig. 2(a). Due to the small refractive index contrast, the cavity mode (3) penetrates extensively into the surrounding DBRs, on the order of $\bar{n}/\Delta n \simeq 11$ periods.

4. Results and discussions

Spectroscopic measurements were performed with a modified optical microscope to analyze the optical performance of the DBRs and the cavities at various locations on the films. The sample is broad area illuminated with an incandescent source, and a spectrally-broadband beamsplitter couples a fraction of the light reflected from the sample through a multimode fibre into an Ocean Optics USB4000 spectrometer. The setup is normalised and calibrated using reference mirrors,

#121929 - $15.00 USD Received 23 Dec 2009; revised 27 Jan 2010; accepted 3 Feb 2010; published 17 Feb 2010

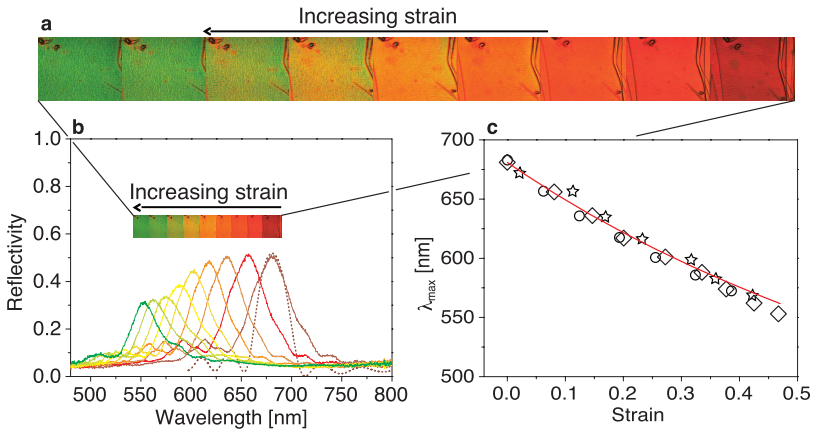

Fig. 3. **DBR tuning. (a)** As the multilayer stack is stretched, the colour changes rapidly and reversibly (image height: 140 μm). **(b)** Reflectivity spectra of the multilayer stack at increasing strains. The dashed line shows the result of a reflectivity calculation for $\varepsilon = 0$. **(c)** Peak wavelength as a function of strain. Circles, diamonds and stars correspond to three consecutive strain cycles. The red line is the prediction of Eq. (4).

with a 10 μm detection spot size used. The samples were stretched in the optical setup using low profile, stepper motor controlled translation stages arranged to compensate any translation in position.

Upon stretching the multilayer sample, the reflectance peak reversibly shifts to lower wavelengths (Fig. 3). The reflectance spectra in Fig. 3(b) were acquired from a 20 layer DBR. The reflectivity peak at wavelength $\bar{\lambda}$, corresponds to predictions of the reflectivity spectrum based on the transfer matrix calculations. Assuming ideal rubber elasticity for both polymers and making use of Eq. (1), the peak wavelength tuning is given by

$$\bar{\lambda}(\varepsilon) = \frac{\bar{\lambda}_0}{\sqrt{1+\varepsilon}} \tag{4}$$

Repeated quasi-static stretching cycles did not alter the zero-strain wavelength of 681 nm $\pm$ 2 nm, nor its variation as a function of strain [Fig. 3c]. The samples therefore exhibited full elastic recovery and the absence of ageing of the multilayer stacks for up to 12 cycles tested here. For the low frequency actuation of this study, the mechanical and optical response was instantaneous. Higher frequency actuation is conceptually limited only by molecular (Rouse) relaxation processes on sub-microsecond time scales [30], but dissipative losses potentially limit practical actuation speeds to less than 1 kHz. While the chemically cross-linked nature of PDMS prevents stress relaxation for static applied stresses, creep has been reported in PSPI if the applied stress exceeded two days at 30 °C [31]. This study would imply that the PSPI used here would creep if stressed for longer than one week at room temperature, but other elastomer systems can give even more stable performance. Higher frequencies actuation is conceptually limited only by molecular (Rouse) relaxation processes on sub-microsecond time scales [30], but dissipative losses of high frequency actuation probably limit actuation to less than 1 kHz. While the chemically cross-linked nature of PDMS prevents stress relaxation for static applied stresses, creep has been reported in PSPI if the applied stress exceeded two days at 30 °C [31]. Based on this study, PSPI of the composition used in this work should exhibit creep only for static applied stresses exceeding one week at room temperature.

#121929 - $15.00 USD Received 23 Dec 2009; revised 27 Jan 2010; accepted 3 Feb 2010; published 17 Feb 2010

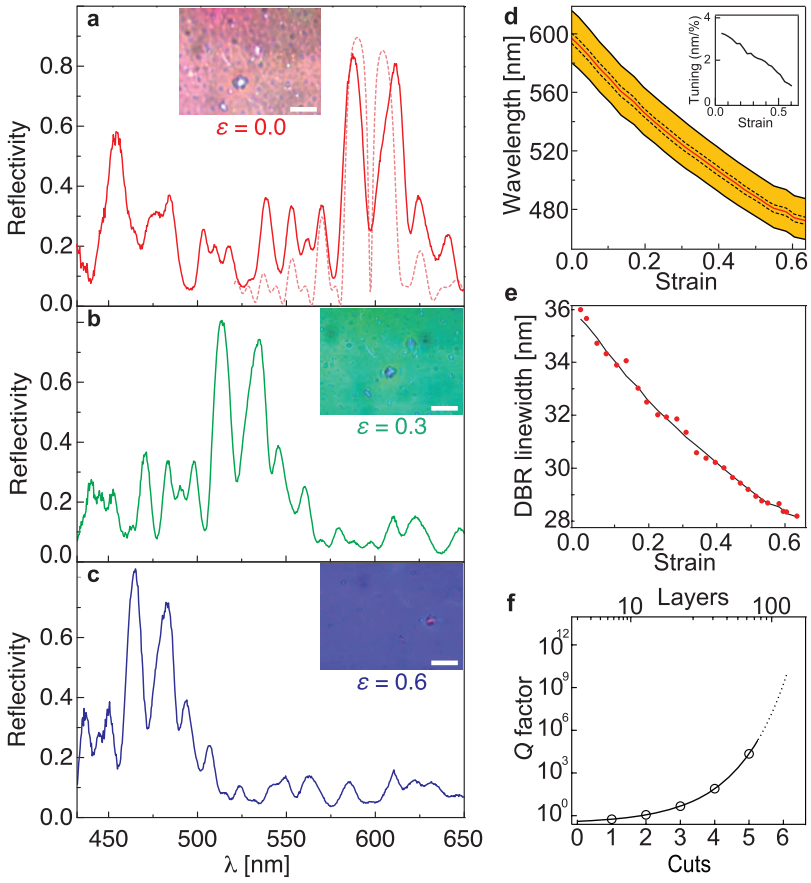

Fig. 4. **Elastomeric microcavity tuning as a function of strain. (a)** $\varepsilon = 0$, **(b)**, $\varepsilon = 0.3$ and **(c)**, $\varepsilon = 0.6$. Insets show micrographs of the film surface in reflection at each strain (scalebar: 20 μm). The dashed line in **(a)** is a calculation for $\varepsilon = 0$. **(d)** DBR mirror stop band (black lines) and microcavity mode (red line) *vs* applied strain. The fits for both are identical and follow equation (4). The inset shows the rate of wavelength change with applied strain. **(e)** DBR bandwidth and fit (line) *vs* applied strain. **(f)** Theroetically predicted *Q*-factor of the microcavities as a function of the number of cut-and-stack operations.

With a refractive index difference of $\Delta n = 0.13$, the maximum DBR reflectivity observed amounts to $\sim 50\%$, which is only slightly less than the 52% predicted by model calculations. The peak width of 50 nm is larger than the 35 nm predicted by theory which is presumably due to imperfections and scattering in the multilayer caused by the current stack manufacture.

The decrease in intensity at higher strains probably arose from two effects : (1) The thinning of the stack at high strains may have moved the film out of the microscope focus, thereby drastically lowering the intensity of the incident light per unit area. (2) Small cracks appeared in this particular sample at strains above 35%, which were not observed in multilayer cavities or multilayer sample with smaller stack numbers. They are a film-preparation artefact which was avoided in subsequent sample preparation.

The optical performance of a fully elastomeric microcavity based on two stretchable DBRs surrounding a $\lambda/2$ PSPI spacer layer is shown in Fig. 4. A clear cavity mode is present in the

#121929 - $15.00 USD Received 23 Dec 2009; revised 27 Jan 2010; accepted 3 Feb 2010; published 17 Feb 2010

middle of the DBR stopband, with the peak reflectivity now increasing to $R_{\max} \approx 85\%$ (compared to a predicted reflectivity of 89%). The change in shape of the cavity dip is minimal upon stretching, with both DBR mirrors and the cavity mode following identical tuning [Fig. 4(d)]. Significantly, the wavelength of the cavity resonance follows Poisson's law [Eq. (4)] very accurately for strains exceeding $\varepsilon = 0.65$, which enables precise tuning of the cavity mode. The absolute reflectivities also do not decrease with stretching, which indicates that the thickness ratio of the PSPI and PDMS layers remains constant. Hence although the mirror bandwidth of these DBRs is five times smaller than their tuning range, the cavity mode remains spectrally aligned with the stopband at all strains [Fig. 4(d)]. This bandwidth is as expected from theory, $\Delta\lambda = \frac{2}{\pi}\lambda\frac{\Delta n}{\bar{n}} \simeq 35\,\text{nm}$ at low strain, and decreasing as predicted on stretching [Fig. 4(e)] [28]. Wider free spectral ranges can be achieved by increasing the refractive index contrast in the multilayer, for example by doping one of the rubbers with nanoparticles [29].

The quality factor of the cavity $Q \simeq 55$ is independent of the applied strain. Provided the defect density can be limited by minimising the number of floating steps using the "origami", roll-up or "cut and stack" techniques, we emphasise an extremely favourable exponential scaling of the cavity Q with the number of 'cut and stack' operations, c, used in cavity construction, which rapidly increases the number of layers, $N = 2^{c+1}$. For small Δn, the resulting Q-factor increases as

$$Q = Q_0 \exp\left\{2N\frac{\Delta n}{\bar{n}}\right\} \tag{5}$$

where $Q_0 = \frac{m\pi}{4}\left(\frac{n_0}{n_s}\right)$, n_0, n_s are the superstrate and substrate refractive indices, and m is the number of half-wavelengths that fit inside the microcavity [Fig. 4(f)]. While the Q factor of the cavities is not yet very high, the extrapolation of Eq.(5) illustrates the potential of our technique. Cavities with higher Q-factors can be built by improving multilayer manufacture in applying the "Cut and stack", "Roll up" or "Origami" techniques to drastically decrease the number of floating steps, while minimising the inclusion of imperfections. In principle the limit on the optical quality of the cavities is the roughness of the initial bilayer, which can be less than 1 nm, when optimised.

Future study will have to address the maximum number of cycles at high and low frequencies and static stress relaxation. Based on the large body of literature about the two commodity rubbers used in this work, we expect excellent repeatability and reproducibility for a large number of cycles and frequency range. Out limited testing did not reveal any signs of sample delamination or other signs of physics degradation of the rubber multilayers.

5. Future prospects

A straightforward extension of our elastomeric microcavities is the inclusion of a dye within the cavity to manufacture tuneable emitters, in which the output colour is controlled by the local strain, which can be applied by a standard micro-actuator. These optically-pumped polymer cavity LEDs indeed give narrowband enhanced and beamed light emission.

A more intriguing possibility is the creation of stable laterally localised microcavities in which the light is confined in all spatial directions. Normally the production of non-planar DBRs is problematic, particularly on the micrometre length scale [32]. Here we demonstrate a simple cavity confinement by compressing an elastomeric flexible DBR on a stamped PDMS grating (4 μm pitch, 250 nm high square grooves) to create curved DBRs on the wavelength scale (Fig. 5). Subsequent AFM imaging shows that the DBR has a height variation of 30 nm [Fig. 5(b)], which is observed in the transmission intensity through the microcavity [Fig. 5(c)]. The cavity is constructed by spin coating a Teflon AF spacer layer of thickness $\simeq \lambda/2n = 206\,\text{nm}$ on the lower multilayer dielectric DBR, designed so that the optical

#121929 - $15.00 USD Received 23 Dec 2009; revised 27 Jan 2010; accepted 3 Feb 2010; published 17 Feb 2010

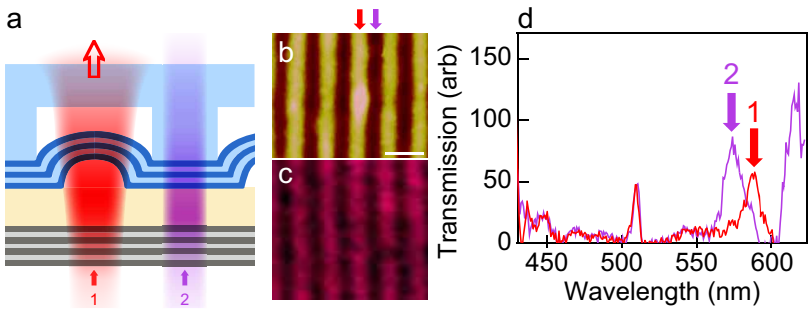

Fig. 5. **Microcavity formed from a flat lower DBR on glass, and an upper elastomeric DBR on a PDMS grating. (a)** Schematic cross-section: a DBR multilayer is placed on a PDMS line grating (pitch: 4 μm, 250 nm high square grooves) and the assembly is put into contact with a commercial planar DBR covered by a 206 nm thick PDMS spacer layer. Stable cavity modes form at position 1. **(b)** AFM image of the elastomeric DBR on the PDMS line grating (height scale: 30 nm, scalebar: 5 μm), and **(c)** transmission image of the full microcavity in IR light. **(d)** Selected transmission spectra from line scans across the sample, showing the different confined optical modes at points indicated by red and purple arrows in **(a)**,**(b)**. The peak at 510 nm originates from a defect in the lower DBR only.

field does not acquire extra reflections from the upper surface. Assembling the full cavity is extremely simple since dust and imperfections, that normally inhibit effective microcavity assembly for small spacings, here only locally push apart the upper and lower DBRs. Away from such local defects the same optical characteristics can be observed all across this sample. Using confocal microscopy we observe the resulting cavity mode, whose resonant wavelength clearly tunes periodically across the grating pattern. In the unstable cavity configuration [the shorter cavity 2 in Fig. 5(a)] the cavity mode blue-shifts as expected, and doubles in linewidth.

We envisage creating sheets of such microcavities by stretching the elastomeric DBR over an array of separately addressable holes to allow for control of individual cavity wavelengths. This enables applications in biosensing, microfluidics, and photonics.

In summary we demonstrate the fabrication of rubber-based, stretchable Bragg mirrors and Bragg microcavity filters by simple, scaleable processing techniques. Upon stretching the devices, the reduction in layer thickness blue-shifts the DBR reflection stopband and the microcavity resonant mode. Shifts in wavelength across the entire visible spectrum are achieved by stretching the devices by more than 60%. Stretch-tuneable DBRs can thus be directly employed for optical stress-strain sensing applications, in LED and lasing applications with broadband emitters to allow for wide range wavelength tuning, and in a host of novel applications.

Acknowledgements

Financial support from EPSRC (EP/G060649/1, EP/E040241, EP/C511786/1) is gratefully acknowledged. MK acknowledges support from DAAD (German Academic Exchange Service) and the Cambridge Newton Trust.

#121929 - $15.00 USD Received 23 Dec 2009; revised 27 Jan 2010; accepted 3 Feb 2010; published 17 Feb 2010